Proceedings of the PRADS2013, pp. 1032~1037
20-25 October, 2013
CECO, Changwon City, Korea

Effect of Ship Speed on Ship's Ice Resistance with Ship's Vertical Motions Included

Xiang Tan[1), 2)], Kaj Riska [1), 3)] and Torgeir Moan[1), 2)]

[1)] Centre for Ships and Ocean Structures, Norwegian University of Science and Technology, Norway
[2)] Department of Marine Technology, Norwegian University of Science and Technology, Norway
[3)] TOTAL S.A. - DGEP/DEV/ED/EC, France

Abstract

In this paper, the relations between ice resistance, ship speed and ship motions are investigated with a numerical model simulating the icebreaking process with ship's motions in 6 degrees of freedom (DOF). The coupled motions of ship are considered in all 6 DOF together with the corresponding environmental forces. The coupling between ship's movement and the breaking of ice is solved step by step with the update of ice edge geometry and ship's kinematics variables. Time series of global ice loads (forces and moments) and ship motions are obtained correspondingly. The effect of ship's vertical motions is studied by comparing results between reduced-order-models and the 6-DOF model with hull speeds and ice thickness being parameters. The numerical model was validated with the Swedish icebreaker Tor Viking II in previous works, and this vessel is used in this paper too as the physical prototype of the case study. Results are compared to full scale data as well as Lindqvist's empirical formula.

Keywords

Numerical model; level ice; ice resistance; hull speed; ship motions

Introduction

The influence of ship's forward speed on the ice resistance that the ship experiences during icebreaking process is an important subject for the design of icebreakers. For fixed structures, model- and full-scale tests have been done extensively for the evaluation of speed effect of ice loading. The dependency of global ice load on the ice sheet indenting speed has been widely discussed especially for simple structural forms (e.g., piles and walls, and cones). For moving structures, however, more uncertainties arise due to motions of structures and the consequential interactions between moving structures and ice. For a ship breaking ice continuously, its bow has to open a channel that is sufficiently wide for the whole beam to transit through. The channel opened by the ship is composed of repeated breaking and clearing cycles of ice edge. Since the breaking (the floe size and the failure load) of individual ice wedge is dependent on the local loading conditions (loading rates and friction, etc.), ice properties and hull forms, the icebreaking pattern formed by the bow will not just influence hull motions but be a consequence of ship's motions.

Previously, a numerical model simulating ship's operations in level ice with six degrees of freedom (DOFs) was developed at CeSOS, NTNU (Tan et al., 2013). The physical processes occur during icebreaking by ships are modeled by combination of theoretical analysis and empirical method. Results were obtained in time domain and validated with full scale data for full-propulsion performance. In the present work, modification to the predefined breaking manner is made by introduction of an additional empirical coefficient, C_r , accounting for the broken ice floe aspect ratio. Moreover, the dynamic bending effect of loaded ice edge is incorporated into the numerical procedure. Based on the dynamic response of the loaded ice sheet, numerical experiments are carried out with five hull speed values ranging from 1.0m/s to 9.0m/s. For each of the hull speeds, three motion configurations, i.e., 6-DOF, planar and fixed-hull models, are calculated for ice thicknesses between 0.1m and 1.1m.

Numerical Model

Kinematics

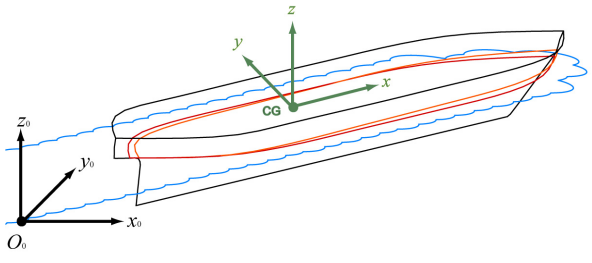

Fig. 1: Reference Frames

Ship's state variables, forces and the geometries of ship and ice edge are expressed with respect to two right-handed Cartesian reference frames illustrated in Fig. 1.

The global position and orientation of the ship as well as the level ice sheet is defined in the earth-fixed, inertial frame, denoted as $\boldsymbol{x}_0\boldsymbol{y}_0\boldsymbol{z}_0$. The coordinate plane $\boldsymbol{x}_0\boldsymbol{O}_0\boldsymbol{y}_0$ coincides with the calm water plane. The axis $\boldsymbol{O}_0\boldsymbol{z}_0$ points upward.

Ship's state variables, i.e., velocities and accelerations, are defined in the reference frame that is moving and rotating along with the ship, i.e., the body-fixed frame, denoted as ***xyz***, whose coordinate axes are parallel to the principal axes of inertia of the ship (Fig. 1). The origin is set to be at the center of gravity (CG) of the ship. Equations of motions for the ship are solved in the body-fixed frame.

Kinetics

The equations of motions for the ship could be expressed in vector form as:

$$(\mathbf{M}+\mathbf{A})\ddot{\mathbf{r}}+\mathbf{B}\dot{\mathbf{r}}+\mathbf{C}\mathbf{r}=\mathbf{F} \tag{1}$$

where **M**, **A**, **B** and **C** are the general mass, added mass, damping and restoring force matrices.

For a model with ship motions in six degrees of freedom, the state variables, $\ddot{\mathbf{r}}$, $\dot{\mathbf{r}}$, $\mathbf{r}$, and excitation, **F**, are vectors with six elements arranged in the order of surge, sway, heave, roll, pitch and yaw:

$$\begin{aligned}\ddot{\mathbf{r}}&=[\dot{u},\dot{v},\dot{w},\dot{p},\dot{q},\dot{r}]\\ \dot{\mathbf{r}}&=[u,v,w,p,q,r]\\ \mathbf{r}&=[x,y,z,\phi,\theta,\psi]\end{aligned} \tag{2}$$

and

$$\mathbf{F}=[F_x,F_y,F_z,M_x,M_y,M_z] \tag{3}$$

where the first three components are translational and the last three are rotational.

It is assumed that the total excitation force (Moments) exerted on the ship is able to be broken down into several components associated with different physical processes that occur during icebreaking:

$$\mathbf{F}=\underbrace{\mathbf{F}^{\mathrm{sbmg}}+\mathbf{F}^{\mathrm{brk}}}_{\mathbf{F}^{\mathrm{ice}}}+\mathbf{F}^{\mathrm{p}}+\mathbf{F}^{\mathrm{ow}} \tag{4}$$

where $\mathbf{F}^{\mathrm{ice}}$ is the total ice resistance composed of a component, $\mathbf{F}^{\mathrm{sbmg}}$, for clearing and submerging the broken ice floes, and a component, $\mathbf{F}^{\mathrm{brk}}$, arises from breaking of intact ice. $\mathbf{F}^{\mathrm{p}}$ is the propeller and rudder force; $\mathbf{F}^{\mathrm{ow}}$ is the open water resistance.

The excitation defined in Eq. (4) is calculated at each time step, and the equations of motions are solved by assuming a linear variation of acceleration during one time step. Since $\mathbf{F}^{\mathrm{brk}}$ and ship's position are coupled, iterations are performed in each time step to achieve equilibrium. The ship's state variables and ice edge are updated at the end of each time step. A more detailed solving procedure is stated in Tan et al. (2013).

In the present work, the icebreaking force component, $\mathbf{F}^{\mathrm{brk}}$, is modeled based on the geometry of contact and relative motions between the ship hull and the ice edge at each time step. The modeling method will be introduced briefly in the following sections.

As for other components, $\mathbf{F}^{\mathrm{sbmg}}$ is calculated based on Lindqvist's resistance formula (Lindqvist, 1989); $\mathbf{F}^{\mathrm{ow}}$ is calculated by cross-flow theory (Faltinsen, 1990).

Geometry Model

The geometries of ship hull and ice edge are numerically modeled by adjacent nodes and line elements and are updated in accordance with ship motions for every new time step. Since the ship hull at waterline is crucial for the breakage of ice, the portion around the icebreaking waterline is extracted for the ship-ice contact algorithm (Fig. 2). An auxiliary waterline several millimeters below the icebreaking waterline is additionally generated to help construct hull panels for the determination of frame angles (φ) at each hull node location.

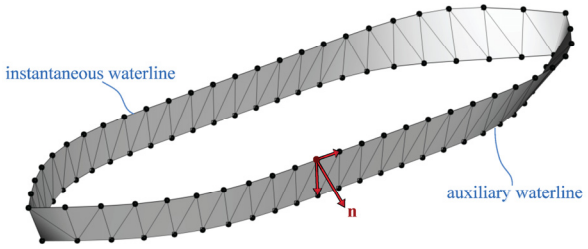

Fig. 2: Modelling Hull Form at the Waterline

The contact regions between ship and ice are detected geometrically at each time step by a contact algorithm (Fig. 3). The area of each contact surface, A_{cr}, is then calculated with the frame angle and depth of indentation at the corresponding location.

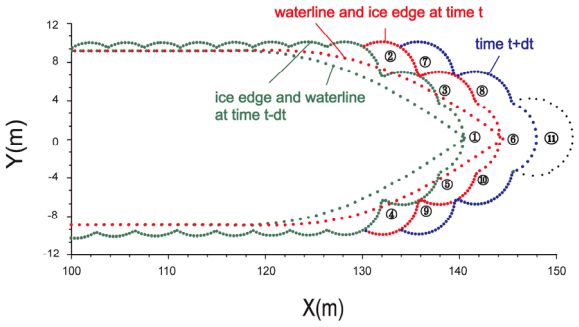

Fig. 3: Nodal Contact Model

Contact Forces

The local contact forces (Fig. 4), i.e., the initial crushing and icebreaking forces, on each of the contact regions are then calculated by the relationships given by Eq. (5) through Eq. (7):

$$F_{cr}=\begin{cases}-p_{av}A_{cr}, & v_2\le 0\\ 0, & v_2>0\end{cases} \tag{5}$$

$$f_1 = \mu F_{cr} \frac{v_1}{\sqrt{v_\tau^2 + v_1^2}} \tag{6}$$

and

$$f_\tau = \mu F_{cr} \frac{v_\tau}{\sqrt{v_\tau^2 + v_1^2}} \tag{7}$$

where p_{av} is the average crushing pressure on the contact surface; F_{cr} is the normal contact force caused by the normal relative velocity v_2; f_1 and f_τ are components of frictional force caused by the relative sliding velocities v_1 and v_τ in the contact plane.

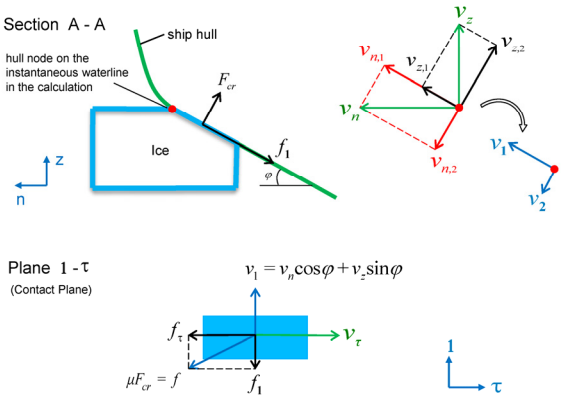

Fig. 4: Local Contact Forces on Ship

The local contact forces are then transformed into the body-fixed frame and integerated along the waterline to obtain the sum icebreaking force acting on the ship.

Icebreaking Pattern

It is observed in full-scale as well as model-scale tests that the loaded ice edge by an icebreaker in advancement fails with the formation of a circumferential crack, as is depicted in Fig. 3. Full- and model-scale tests also suggested that the size of the broken floe increases with increasing ice thickness (h_i) and decreases with increasing hull speed (Lewis et al., 1970; Varsta, 1983). In this paper, the size of the broken ice floe is determined by a breaking radius proposed in Wang (2001):

$$R = C_l l_c (1 + C_v v_2) \tag{8}$$

and a floe width to depth ratio, C_r, based on full scale report given in Milano (1973). In Eq. (8), C_l and C_v are empirical constants associated with the characteristic length of ice, l_c, and the normal impact speed v_2.

Model Configurations

The numerical model is designed with ship motions in six DOFs. By constraining any of the DOF(s), reduced-order models can be generated to realize captive and free run operations. In this paper, the numerical results are presented with

- 6-DOF model;
- Planar model (3-DOF model), with ship motions in surge, sway and yaw;
- Fixed-hull model, with ship motion in surge direction only.

Influence of ship motions on ice resistance are then investigated with a series of hull forward speed.

Case Study

Ship's Main Particulars and Ice Properties

The Swedish Icebreaker Tor Viking II is adopted as physical prototype in the case study. More detailed information on ship's operation conditions is introduced in Riska et al. (2001). The primary ship and ice parameters are listed in Tables 1~2.

Table 1: Ship's Particulars

Parameter	Notation	Value	Dimension
Length over all	LOA	83.70	m
L. between perpendiculars	Lpp	75.20	m
Breath, moulded	B	18.00	m
Draught, max icebreaking	D	6.50	m
Propulsion output	PD	13440	kW
Open water speed	vow	16.40	knot

Table 2: Ice Material Properties

Parameter	Notation	Value	Dimension
Density	ρ_i	880	kg/m3
Young's modulus	E	5.40×109	Pa
Poisson ratio	ν	0.33	
Crushing strength	σ_{cr}	2.30×106	Pa
Bending strength	σ_f	0.58×106	Pa
Frictional coefficient	μ	0.15	

Ship's Performance

The simulated ship speeds at full power during steady state are plotted in Fig. 5. The numerical results generally agree well with the regression curve of full-scale data. Speeds calculated by the 6-DOF model are slightly higher than other models in most cases. This is attributed to the fact that relieving artificial constraints on the vertical DOFs is beneficial to breaking of ice since more velocity components have participated in determining the loading rates (Tan et al., 2013). It is also noted from

Fig. 5 that in thick ice, the speeds from fixed-hull model are higher than those from the planar model by a small amount. The reason could be that transverse motions such as sway and yaw under some conditions cause an additional resistance and this will be furtherly discussed in the following sections.

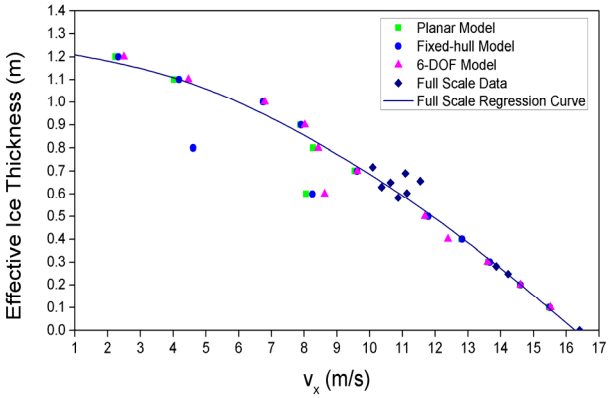

Fig. 5: *h-v* Curve

Time Series of Ship Motions and Resistances

An example of the simulated motions and icebreaking force and moments are presented in Fig. 6 and 7.

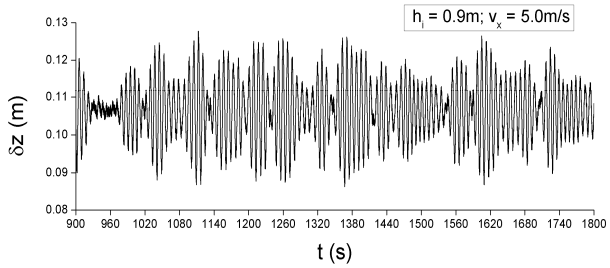

(a) Heave

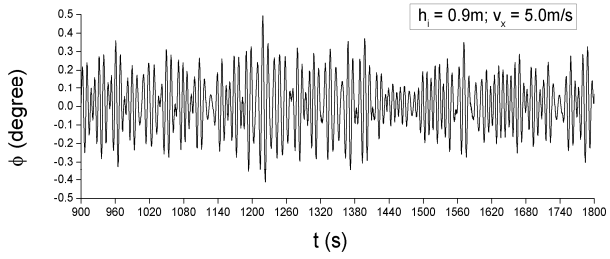

(b) Roll

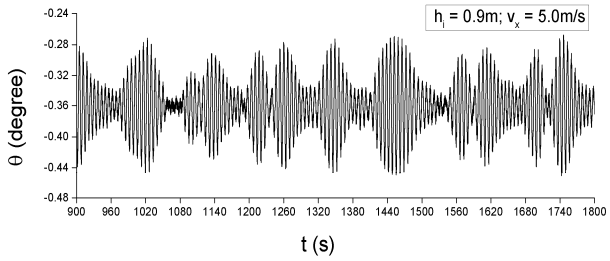

(c) Pitch

Fig. 6: Simulated Ship Vertical Motions (h_i = 0.9m; v_x = 5.0m/s)

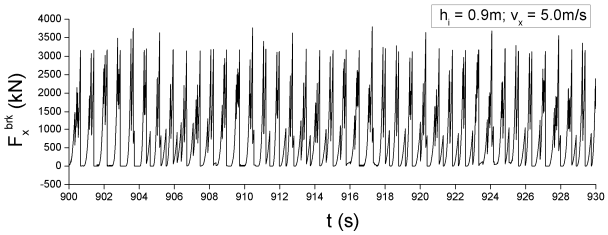

(a) Icebreaking Resistance (surge)

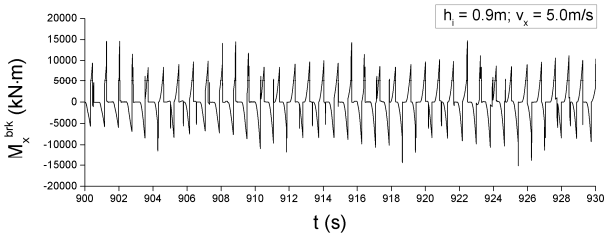

(b) Roll Moment from Icebreaking

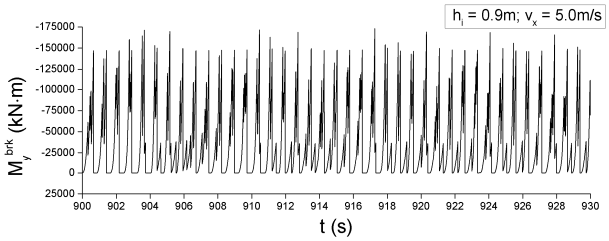

(c) Pitch Moment from Icebreaking

Fig. 7: Simulated Ice Resisting Force and Moments from Icebreaking (h_i = 0.9m; v_x = 5.0m/s)

Influence of Hull Speed on Ice Resistance

The dependencies of ship's ice resisting force and moment on forward speed is depicted in Fig. 8, where the Lindqvist's predictions are also marked for the surge resistance. A distinct linear relationship is observed for the numerical results, which agrees with most of the empirical formulae. The numerical model comparing to the Lindqvist's resistance formula gives higher ice resistance values.

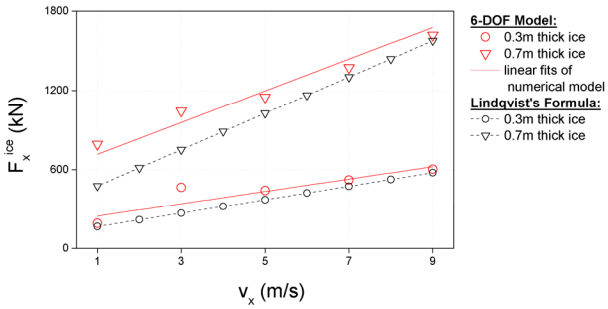

(a) Ice Resistance vs. Hull Speed

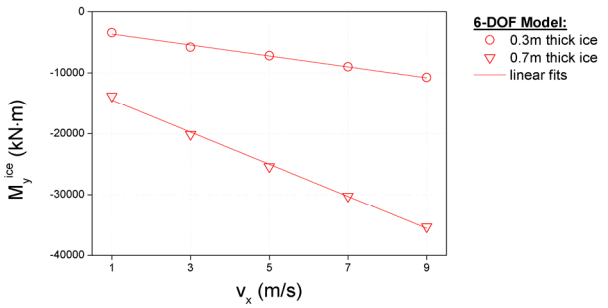

(b) Pitch Moment from Ice vs. Hull Speed

Fig. 8: Ice Resisting Force and Moment vs. Hull Speed

Influence of Ship Motions on Ice Resistance

The simulated ship's ice resistance for a series of hull speeds is shown in Fig. 9. In Fig. 9(a), results from 6-DOF model and planar model are presented. For cases with thin ice (0.1m and 0.3m), the resistance given by the two motion configurations are quite close. As the ice becomes thicker, that the planar model tend to give a much higher ice resistance than the 6-DOF model is more obvious. This is attributed to the influence of vertical motions (heave, pitch) which could under certain circumstances alter the icebreaking pattern which would influence the resistance that the ship experiences (Tan et al., 2013).

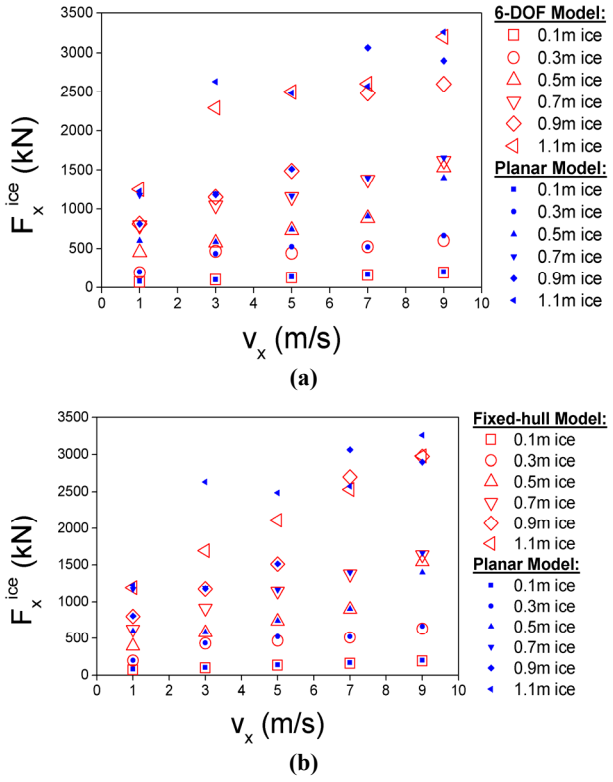

Fig. 9: Dependencies of Ice Resistance on Ship's Forward Speed for Different Model Configurations (Ice Thickness as Parameter)

Fig. 9(b) compares the simulated results from the fixed-hull model and the planar model. The comparison between these two motion configurations implies that lateral motions (sway, yaw) bring an additional resistance, which could under certain conditions be significant, due to the enlarged forward projected area and frequent crushing by the side hull. Take the h_i = 0.9m, v_x = 5.0m/s case for example, the simulated icebreaking patterns are depicted in Fig. 10. In Fig. 10(a), the bow opens a channel that is wide enough for the whole ship to pass through; no side contact is detected in the mid-body regions where the slope of the ship hull is close to vertical. As is shown in Fig. 10(b), however, sway and yaw lead to constant contact (crushing) between the side hull and the channel edge which results in a larger resistance especially when the channel opened by the bow is not sufficiently wide.

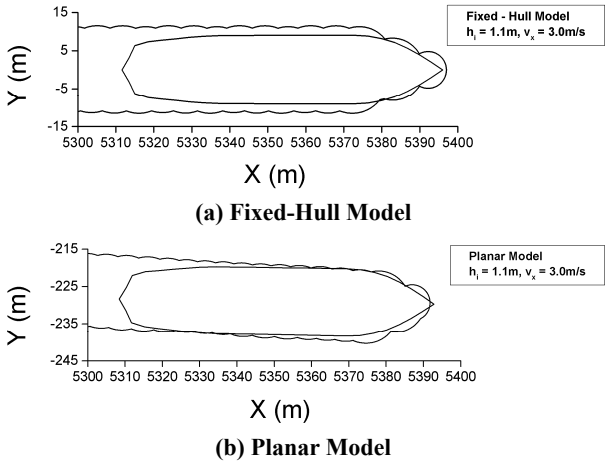

Fig. 10: Simulated Icebreaking Patterns from Two Motion Configurations (h_i = 1.1m; v_x = 3.0m/s)

In Fig. 11 the ice resisting pitch moment from the 6-DOF model is shown together with the pitch restraining moment from the fixed-hull model. The pitch restraining moment is higher than the pitch resisting moment for thick ice. This again implies that the relieved degrees of freedom, notably heave and pitch, are beneficial to breaking of ice and result in a lower ice resisting force (moment).

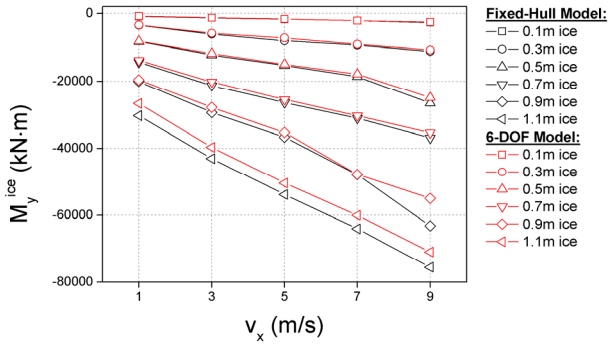

Fig. 11: Comparison between Ice Resisting Moment (6-DOF Model) and Motion Restraining Moment (Fixed-Hull Model) in Pitch

Conclusions

The effect of hull speed on ship's ice performance and resistance is investigated with a previously developed numerical model simulating ship motions in level ice with six degrees of freedom. Case studies are carried out with several ice thicknesses and ship's hull speeds for three motion configurations. The main conclusions are as follows:

- The dependency of ship's ice resistance (surge and pitch) on hull speed is observed to be linear as is predicted by Lindqvist's empirical formula;
- Pitch and heave would under some circumstances alter the icebreaking pattern which would lower the resistance that the ship experiences;
- Sway and yaw under some conditions bring an additional resistance to the ship due to an enlarged forward projected area which cause more frequent side contact between the ship and ice edge.

Acknowledgement

The authors would also like to acknowledge TOTAL E&P NORGE AS and the Research Council of Norway through the Centre for Ships and Ocean Structures in Norwegian University of Science and Technology for funding of the research.

References

Faltinsen, O.M. (1990). "Sea loads on ships and offshore structures", Cambridge University Press, Cambridge, UK.

Lewis, J.W. and Edwards R.Y. (1970). "Methods for predicting icebreaking and ice resistance characteristics of icebreakers", Transactions of Society of Naval Architects and Marine Engineers (SNAME), Vol. 78, pp. 213-249.

Lindqvist, G. (1989). "A Straightforward Method For Calculation of Ice Resistance of Ships", Proc. 10th International Conference on Port and Ocean Engineering under Arctic Conditions (POAC), Luleå, Sweden. pp. 722–735.

Milano, V. (1973). "Ship resistance to continuous motion in ice". Transactions of Society of Naval Architects and Marine Engineers (SNAME), No. 9.

Riska, K., Leiviskä, T., Fransson, L., etc., 2001. Ice performance of the Swedish multi-purpose icebreaker TOR Viking II, Proc. 16th International Conference on Port and Ocean Engineering under Arctic Conditions (POAC), Ottawa, Canada. pp. 849-866.

Tan, X., Su, B., Riska, K. and Moan, T. (2013). "A Six-Degrees-of-Freedom Numerical Model for Level Ice-Ship Interaction", Cold Regions Science and Technology. Accepted.

Varsta, P. (1983). "On the mechanics of ice load on ships in level ice in the Baltic Sea". Ph.D. Thesis, Helsinki University of Technology, Espoo, Finland.

Wang, S. (2001). "A dynamic model for breaking pattern of level ice by conical structures", Ph.D. Thesis, Department of Mechanical Engineering, Helsinki University of Technology, Espoo, Finland.